Steel and Composite Structures, *Vol. 36, No. 4 (2020) 399-415*
DOI: https://doi.org/10.12989/scs.2020.36.4.399

Evaluation of responses of semi-rigid frames at target displacements predicted by the nonlinear static analysis

Vijay Sharma *[1], Mahendra K. Shrimali[2a], Shiv D. Bharti[2b] and Tushar K. Datta[2c]

[1]*Department of Civil Engineering, Malaviya National Institute of Technology Jaipur, JLN Marg, Jaipur 302017, India*
[2]*National Centre for Disaster Mitigation and Management, Malaviya National Institute of Technology Jaipur, JLN Marg Jaipur, 302017, India*

(*Received February 3, 2020, Revised July 6, 2020, Accepted July 24, 2020*)

Abstract. Responses of semi-rigid frames having different degrees of semi-rigidity obtained by the nonlinear static analysis (NSA) are evaluated at specific target displacements by comparing them with those obtained by the nonlinear time-history analysis (NTHA) for scaled earthquakes. The peak ground accelerations (PGA) of the earthquakes are scaled such that the obtained peak top story displacements match with the target displacements. Three different types of earthquakes are considered, namely, far-field and near-field earthquakes with directivity and fling-step effects. In order to make the study a comprehensive one, three degrees of semi-rigidity (one fully rigid and the other two semi-rigid), and two frames having different heights are considered. An ensemble of five-time histories of ground motion is included in each type of earthquake. A large number of responses are considered in the study. They include the peak top-story displacement, maximum inter-story drift ratio, peak base shear, total number of plastic hinges, and square root of sum of the squares (SRSS) of the maximum plastic hinge rotations. Results of the study indicate that the nonlinear static analysis provides a fairly good estimate of the peak values of top-story displacements, inter-story drift ratio (for shorter frame), peak base shear and number of plastic hinges; however, the SRSS of maximum plastic hinge rotations in semi-rigid frames are considerably more in the nonlinear static analysis as compared to the nonlinear time history analysis.

Keywords: NSA; NTHA; semi-rigid frame; near-field; far-field; seismic performance; target displacement

1. Introduction

Because of the higher ductility, steel buildings perform better during severe earthquakes as compared to concrete buildings. The efficacy of these buildings can be improvised by adopting moment resisting frames (MR), especially for high seismic prone areas. These frames are generally designed considering the capacity-design concept, which means these follow the strong column-weak beam design concept. The famous 1994 Northridge and 1995 Kobe earthquakes revealed the seismic vulnerability of rigid moment frames designed with the above concept. In the extreme shaking, the rigid beam-column connections were found to be severely damaged. These observations led to the development of semi-rigid connections. The seismic performances of rigid and semi-rigid MR frames were investigated in the past by various researchers both experimentally and analytically (Nader and Astaneh 1991, Elnashai and Elghazouli 1994, Awkar and Lui 1999, Silva *et al.* 2018). These studies revealed the efficacy of the partially restrained or semi-rigid (SR) connections in the form of its ductile nature and the use of lighter flexural sections to meet the strong column-weak beam needs (Aksoylar *et al.* 2011).

In the last two decades, extensive research has been carried out to assess the dynamic behavior of SR frames. The earlier investigations (Al-Bermani *et al.* 1994, Lui and Lopes 1997, Chan and Chui 2000) have demonstrated that the stiffness of the connection altered the dynamic characteristics of frames, especially increasing the natural period of vibration. The behavior of seismically protected steel rigid frames subjected to the near-field pulse-type motion under different scenarios has been investigated by several researchers (Foti 2014, Foti 2014, Foti 2015, Abdollahzadeh *et al.* 2016, Diaferio and Foti 2016, Diaferio 2018). However, the same for the semi-rigid frame is scanty. Faridmehr *et al.* (2016) studied the competence of SR connections based on ANSI 360-10 and Eurocode 3 Part 1-8 (Eurocode 3 2006) provisions to maintain the desired strength, stiffness, and ductility parameters of the structural system. Feizi *et al.* (2015) and Bayat and Zahrai (2017) investigated the enhanced seismic performance by employing the optimal locations of the SR connection in hybrid frames. Faridmehr *et al.* (2017) proposed a nonlinear stiffness matrix method to evaluate the seismic response of semi-rigid steel frames under a set of earthquakes. Recently, few researchers investigated the performance of moment

*Corresponding author, Ph.D. Student
E-mail: vrsgec2011@gmail.com
[a]Professor
E-mail: shrimalimk@gmail.com
[b]Professor
E-mail: sdbharti@mnit.ac.in
[c]Professor
E-mail: tushar_k_datta@yahoo.com

http://www.techno-press.org/?journal=scs&subpage=8
ISSN: 1229-9367 (Print), 1598-6233 (Online)

resisting SR frames and found that SR connections exhibit stable hysteretic behavior and high ductility so that they can dissipate the huge amount of seismic energy in joints and beams together (Lemonis 2018, Sharma *et al.* 2018, Sharma *et al.* 2019). Sharma *et al.* (2020) investigated the effectiveness of semi-rigid frames as compared to rigid frames under the near- and far-field earthquakes using nonlinear time history analysis.

The seismic behavior of rigid frames has been extensively investigated using both nonlinear time history analysis (NTHA) and nonlinear static pushover analysis (NSA) (Bracci *et al.* 1997, Mwafy and Elnashai 2001, Kunnath and Kalkan 2004). The validity of predictions by the NSA for rigid frames has also been tested under different conditions by NTHA (Hasan *et al.* 2002, Antoniou and Pinho 2004, Kalkan and Kunnath 2006, Kalkan and Kunnath 2007). Further, different load distribution patterns to improve predictions of the NSA have been proposed by various researchers (ATC-40 1996, FEMA-355D 2001, Mwafy and Elnashai 2001, Chopra and Goel 2002, FEMA-440 2005, Kalkan and Kunnath 2007).

The application of the NSA for semi-rigid connected frames are scanty. Hsieh and Deierlein (1991) studied the behavior of SR steel frames for static and quasi-dynamic actions using the capacity spectrum method (CSM). The seismic performances of rigid and semi-rigid frames were compared in the context of direct displacement-based or performance-based methodology by a few researchers in the past (Liu *et al.* 2008, Roldán *et al.* 2016, Pirmoz and Liu 2017). In recent years, Brunesi *et al.* (2015) investigated the seismic responses in semi-rigid steel MR frames by high-definition finite element simulations and made a comparison among the conventional pushover analysis (POA), adaptive POA, and incremental dynamic analysis. Krolo *et al.* (2015) investigated the seismic performance of semi-rigid steel frames through nonlinear static pushover analysis based on the N2 method.

The aforementioned researches mostly discussed the seismic performances of the rigid and SR frames comparing the seismic demands obtained from the NTHA and NSA at a single performance state for the design level or extreme level earthquake using a limited number of response quantities. Further, these studies did not focus on the target displacement approach. The target displacement (i.e., peak top-story displacement) based comparison between the seismic demand parameters obtained from the NTHA and NSA was earlier investigated by a few researchers (Kalkan and Kunnath 2007, Erduran 2008, Bhandari *et al.* 2018) on rigid and base-isolated frames. The target displacement-based study provides a fair estimate to designers of the expected peak top-story displacement considering the desired PGA of earthquakes and ductility of structures. For rigid frames, the prediction of the NSA at the target displacement (T_d) level has been tested against the NTHA by various techniques. Out of these, the spectral matching and PGA matching techniques have been widely used. The review of the literature clearly indicates that more extensive studies are required to assess the performance of SR frames at different target displacements covering the elastic to the plastic state of the frame as determined from the NSA, especially for near-field earthquakes.

In the presented paper, the PGA matching technique is employed to validate the predictions of the NSA at different target displacements by the NTHA for semi-rigid frames. PGA matching technique consists of scaling the PGA of the earthquake such that the peak top story displacement obtained by the NTHA matches the desired target displacement. The validity of the predictions of the NSA is investigated for different degrees of the semi-rigidity, type of earthquakes (far-field and near-field), and different target displacements (covering elastic to fully plastic state). In order to make the study a comprehensive one, three degrees of joint stiffness or semi-rigidity (one fully rigid and two semi-rigid), three types of earthquakes, namely, the far-field (FF), near-field with directivity (NF-D) and with fling step effects (NF-F), three different levels of target displacements, namely, those at the elastic state, elastic-plastic and plastic state and two frames of five-story and ten-story are considered. A large number of seismic responses are used for comparing the predictions of the NSA with those of the NTHA, namely, the maximum inter-story drift ratio (IDR_{max}), peak top-story displacement (PSD), peak base shear (BS_{peak}), total number of plastic hinges, and their SRSS of maximum plastic hinge rotations. The measure of comparison is taken as the root mean square value of differences between the two sets of responses.

2. Modelling and analysis

This section covers the appropriate modelling of the semi-rigid (SR) connection and its implementation in the standard software SAP2000. Two analysis procedures, namely, the nonlinear static analysis (NSA) and nonlinear time-history analysis (NTHA) are also briefly described.

2.1 Implementation of the appropriate Semi-rigid connection model in SAP2000

The SR connection characteristics are basically dependent on three parameters, namely, the structural stiffness, flexural strength, and ductility of the connecting members. These three parameters define the moment-rotation characteristic curve of the SR connection. The SR connection parameters for the beam-column connection are taken from ANSI 360 (2016) (*See Fig. C-B3.3 of ANSI 360-16*), and the seismic reinforcing requirements for special moment resisting frames are as per the ANSI 341 (2016) recommendations. The generic plot, as shown in Fig 1(a), for all SR connections implemented in SAP2000 has some specific considerations, namely, (i) the yield-moment capacity of the connection ($M_{y,c}$) is selected as the 2/3 of the plastic moment capacity of the connection ($M_{p,c}$), and (ii) the connection flexural strength at the face of the column should not be lower than 0.2 times the plastic moment capacity of the adjoining beam ($M_{p,b}$). The degree of semi-rigidity in the connection is defined by two parameters, α (stiffness parameter) and β (strength parameter), and the connection ductility. The parameters, α, and β, are defined

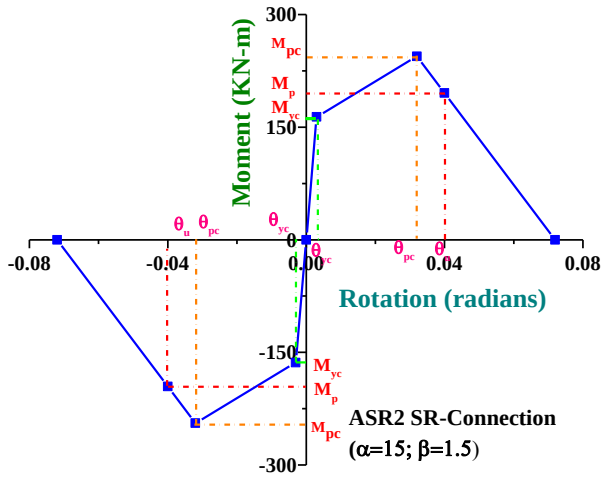

(a) Moment-Rotation backbone curve

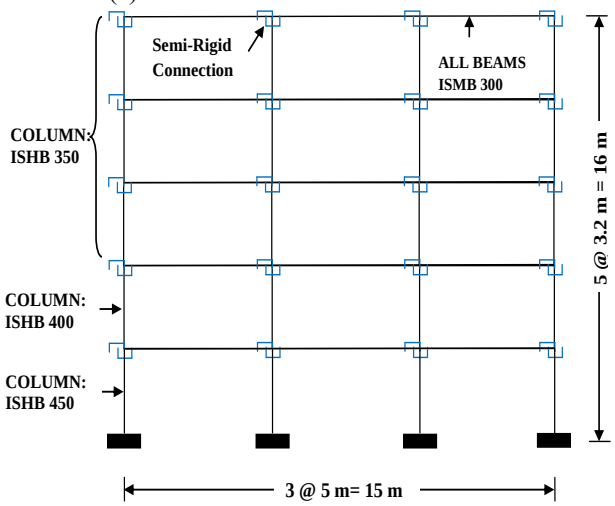

(b) Elevation of the 5-Story semi-rigid frame

Fig. 1 Detailing of the 5-Story semi-rigid frame

in Eqs. 1(a) and 1(b).

$$\alpha = \frac{S_i}{\frac{EI_b}{L_b}} \tag{1a}$$

$$\beta = \frac{M_{p,c}}{M_{p,b}} \tag{1b}$$

where S_i is the initial stiffness, EI_b/L_b is the flexural rigidity of adjoining beam elements.

The ductility parameters are based on the story drift limit. Chan and Chui (2000) suggested that the minimum drift limit 'θ_u' should be more than 0.04 rad for ductile connections. Thus, the peak rotation '$\theta_{p,c}$' of the SR connection is taken as 0.8 times the ultimate rotation 'θ_u.' The linear expansion of the strength degradation beyond 80% reaches to the maximum value of 0.072 radian at which the connection loses its strength near to zero.

The SAP2000v21 (2019) provides two types of beam-column connection link elements, namely, the multilinear elastic link, and multilinear plastic link. Here, the two jointed zero-length multilinear plastic link element (ML-P) with the connection rotational nonlinearity is chosen for the SR connection modeling. The ML-P links are inserted at beam ends only as shown in Fig. 1(b). In Fig 1(b), the cross-sections ISHB and ISMB refer to the Indian Standard column and beam sections respectively. For the 5-Story and 10-Story frames, the details of the cross-sections used are given in Section 3 (Table 1). The ML-P link element exhibits the kinematic hysteretic behavior for the cyclic loading for SR connections implemented in the building frame.

2.2 Nonlinear Static Analysis (NSA)

The nonlinear static analysis (NSA) is a promising technique, especially for designers, to evaluate the seismic response of multi-story MR frame structures. The NSA procedure is simple and requires less computational effort. The efficacy of the NSA procedure is primarily dependent on the lateral load pattern adopted for the analysis. If the structure vibrates primarily in the first or fundamental mode, then the lateral load pattern corresponding to the first mode produces a good estimate of the seismic demands using the CSM method. If the higher modes are predominant or participating considerably, the pushover analysis with other load patterns like the adaptive pushover, multimodal pushover, as discussed in the literature, are used. In the present study, the conventional first mode based lateral load pattern for the NSA is considered to determine the capacity curve or pushover curve of the fully rigid and semi-rigid (SR) frames. In the existing literature on the NSA, many load patterns have been adopted to obtain the capacity curves for the best prediction of responses (Chopra and Goel 2002, Antoniou and Pinho 2004, Kalkan and Kunnath 2006, Kalkan and Kunnath 2007, Poursha and Amini 2015). The results of the study show that there is no unique load pattern which provides the best prediction of responses by the NSA. It depends upon the structure and its configuration including the properties. Since the main objective of the present study is not to find the best load pattern to be adopted for the NSA of SR frames, the conventional fundamental load pattern has been adopted here to obtain the responses by the NSA. However, it may be noted that a comparative study on the responses obtained by a few selected load patterns used in the NSA of SR frames showed that the predictions of responses using the conventional fundamental load pattern are fairly good (Sharma *et al.* 2019). For the conventional fundamental mode shape-based lateral load pattern, the load is monotonically escalated till the monitored target displacement, i.e., 4% of the building height. Iterations may be required at displacement increments in which new plastic hinges are formed.

2.3 Nonlinear-time history analysis (NTHA)

Nonlinear time-history analysis (NTHA) is performed to evaluate the realistic seismic behavior of structures. In previous studies (Reyes and Kalkan 2012), it was shown that the accuracy of the NTHA prediction increased with more number of earthquakes considered in an ensemble of

Table 1 Section detailing of 5-Story and 10-Story building Steel frame

Steel Frame	Story/ Floor	Section (Flexural Member)	h_s (mm)	f_w (mm)	f_t (mm)	t_w (mm)	Story Height	Bay Width	f_y (N/mm^2)	E (N/mm^2)	Poisson ratio
10-Story Steel Frame	1st - 6th	W 14 X 38 (Beam)	358.14	171.96	13.08	7.87	3.2 m	5 m	250	2.10E+05	0.3
	7th -10th	W 14 X 38 (Beam)	358.14	171.96	13.08	7.87	3.2 m	5 m	250	2.10E+05	0.3
	1st - 6th	W 14 X 68 (Column)	353.06	204.72	16.67	9.4	3.2 m	5 m	250	2.10E+05	0.3
	7th -10th	W 14 X 53 (Column)	355.6	254	18.29	10.54	3.2 m	5 m	250	2.10E+05	0.3
5-Story Steel Frame	1st-5th	ISMB 300 (Beam)	300	140	12.4	7.5	3.2 m	5 m	250	2.10E+05	0.3
	1st	ISHB 450 (Column)	450	250	13.5	11.3	3.2 m	5 m	250	2.10E+05	0.3
	2nd	ISHB 400 (Column)	400	250	12.7	9.1	3.2 m	5 m	250	2.10E+05	0.3
	3rd – 5th	ISHB 350 (Column)	350	250	11.6	8.3	3.2 m	5 m	250	2.10E+05	0.3

Note: *h_s= Height of Section; f_w= Flange Width; f_t= Flange Thickness; t_w= Web Thickness; f_y: Steel Grade; E : Modulus of Elasticity*

records, which entail increased computational time. In order to strike a balance between the accuracy and computational time, five number of earthquakes in each ensemble are considered in the study.

The Hilber-Hughes-Taylor direct time integration approach with default parameters (Gamma=0.5 and Beta=0.25) is adopted for the NTHA in SAP2000 software. The 5% Rayleigh proportional damping obtained from the first and second vibration modes are taken for all simulations. The secondary P-delta effects are also considered in the NTHA.

The PGA values for the NTHA simulations are based on the target displacements. The PGA of each earthquake is scaled in such a way that the top story displacements of each frame match with the selected target displacements.

3. Numerical study

Two steel MR frames of five and ten-stories are considered as illustrative examples for the numerical study. Both frames are analyzed and designed with rigid connections using SAP2000 software, satisfying the Indian standard code provisions (IS-875 1987; IS-800 2007). The plan and elevation of the steel frames are shown in Fig. 2 (a) and 2(b). The frames are the typical internal frames of a steel building. The building has a concrete floor slab of thickness 150mm, including floor coating. In addition, dead load comes from the partition wall of thickness 225 mm made by brick masonry. The effective gravity load consists of a dead load of 20 KN/m, a roof dead load of 15 KN/m, and a live load of 4 KN/m uniformly distributed to the beams as shown in the figure. In determining the effective dead load, half of the slab load on either side of the beam is lumped and distributed on the beam. Further, the load of the brick masonry wall is distributed on the beam. Note that the effect of eccentricity is excluded in the determination of loads on the beams of the frame. The steel sections for flexural members are selected to meet the essential requirements of MR frames. For the 5-Story frame, the sections are selected from the Indian Standard Special provision handbook (SP-6-1 2003). For this, the plastic moment capacity of typical columns (***M_p, column***) is taken as 20% more than the plastic moment capacity of the adjoining beams (***$M_{p,b}$***). Thus, the strong column-weak beam (SCWB) capacity design concept is followed, prescribed by the Indian standards. The panel zone is designed with continuity and doubler plates for enhanced capacity to keep the zone in the elastic range. The section details are shown in Table 1.

Both frames are seismically designed as per IS-1893 (2016) requirements. The important seismic design parameters, namely, the PGA level of 0.36g, seismic zone V (severe seismicity Z=0.36), medium soil condition, structure importance factor (I=1), and response reduction factor for special MR frames (R=5) are considered. The semi-rigid frames have the same beam and column sections as those of the rigid frames except for the joint connections. In order to assess the effect of the degree of semi-rigidity, two degrees of semi-rigidity are considered for each frame. The two degrees of semi-rigidity are taken as SR1 (flexible, α=5, β=1.2) and SR2 (stiff, α=15, β=1.5). The SR frames are designated as ASR1, ASR2, BSR1, and BSR2, where 'A' stands for the 5-Story frame, and 'B' stands for the 10-Story frame. The corresponding rigid frames are designated as AFR and BFR. The specific details of semi-rigid connections are presented in Table 2. The fundamental periods of the first three modes of vibration for 5- and 10-Story fully rigid and semi-rigid frames are shown in Table 3.

Three different types of ground motions, namely, the far-field (FF), near-field with directivity (NF-D), and fling step effect (NF-F) are employed to investigate the seismic response at the three levels of target displacements selected. The near-field earthquakes (with directivity and fling step effects) are characterized based on Joyner Boore distance (Rjb < 15 Km) and the far-field earthquake records are chosen from (FEMA-P695 (2009)) document. The near-field with the forward directivity records have two-sided long period velocity pulse, and near-field with fling step records have a single velocity pulse. The NF-F also has a high displacement component and static offset in displacement time history, as shown in Fig. 3.

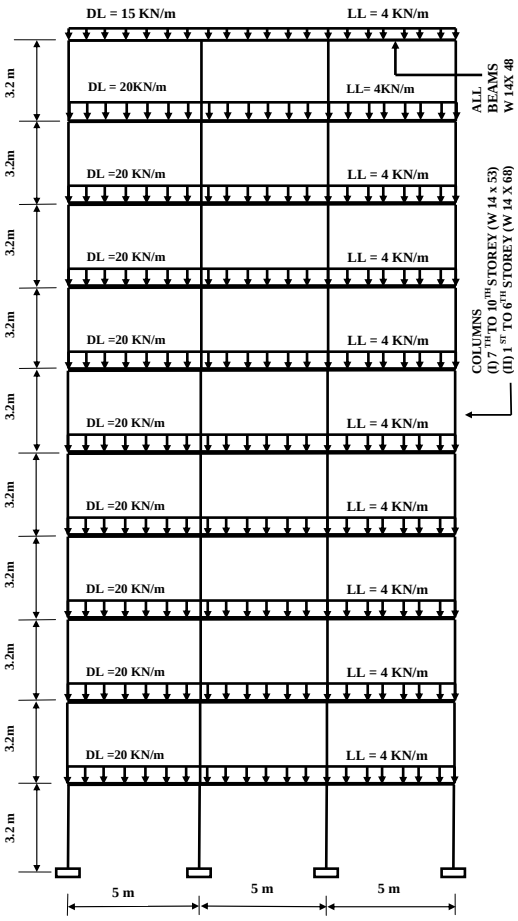

(a) Elevation

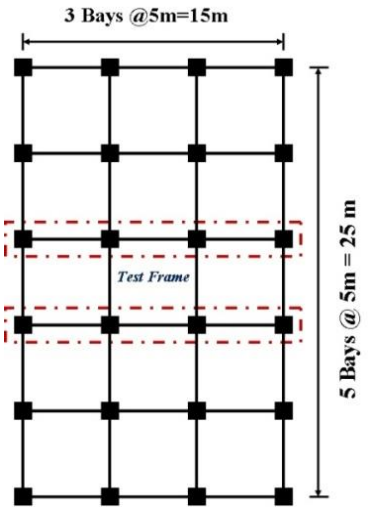

(b) Plan of the building frame

Fig. 2 10-Story rigid frame (a) elevation, (b) plan

A suite of five earthquakes in each type is chosen for the analysis (see Table 4). The time histories of earthquake records are obtained from the PEER ground motion database (PEER 2013). The acceleration response spectra for the far-field and near-field with directivity and fling-step effects are included in Fig. 4.

Table 2 Details of semi-rigid connection modeled in SAP2000

Building	5-Story		10-Story	
Frame ID	ASR1	ASR2	BSR1	BSR2
Stiffness (S_i)	18068	54205	33642	100926
Damping	0.05	0.05	0.05	0.05
M_{yc} (KN-m)	130.99	163.74	202.61	253.26
M_{pc} (KN-m)	195.51	244.39	302.4	378.02
M_p (KN-m)	156.41	195.5	241.92	302.4
θ_{yc} (rad)	0.00725	0.00302	0.00602	0.00251
θ_p (rad)	0.032	0.032	0.032	0.032
θ_u (rad)	0.04	0.04	0.04	0.04

Table 3 The fundamental period of vibrations of rigid and semi-rigid frames

Sr. No	Frame ID	Time Period (Sec)		
		T1	T2	T3
	5-Story Frame			
1	ASR1	1.312	0.385	0.188
2	ASR2	1.143	0.346	0.178
3	AFR	1.033	0.319	0.169
	10-Story Frame			
1	BSR1	2.378	0.758	0.416
2	BSR2	2.032	0.66	0.369
3	BFR	1.825	0.599	0.338

Table 4 Earthquake ground motion records

S.No.	Earthquake-Station (Year)	Magnitude M_w-PGA 'g',	Component
	Far-Field (FF)		
1	Kobe- Nishi-Akashi (1999)	6.9-0.51 g	000
2	Landers- Cool water (1992)	7.3-0.42 g	TR
3	Superstition hill- Poe road-(1987)	6.5-0.45 g	270
4	San Fernando-LA Hollywood	6.6-0.21 g	90
5	Tabas- Ferdows (1978)	7.4-0.093 g	L
	Near-Field Directivity (NF-D)		
1	Erzincan (1992)	6.69-0.5 g	EW
2	Northridge-Sylmar Converter (1994)	6.69-0.83 g	018
3	Kocaeli- Duzce (1999)	7.4-0.31 g	180
4	Imperial Valley-El Centro (1979)	6.53-0.35 g	270
5	Cape Mendocino (1992)	7.00-0.66 g	90

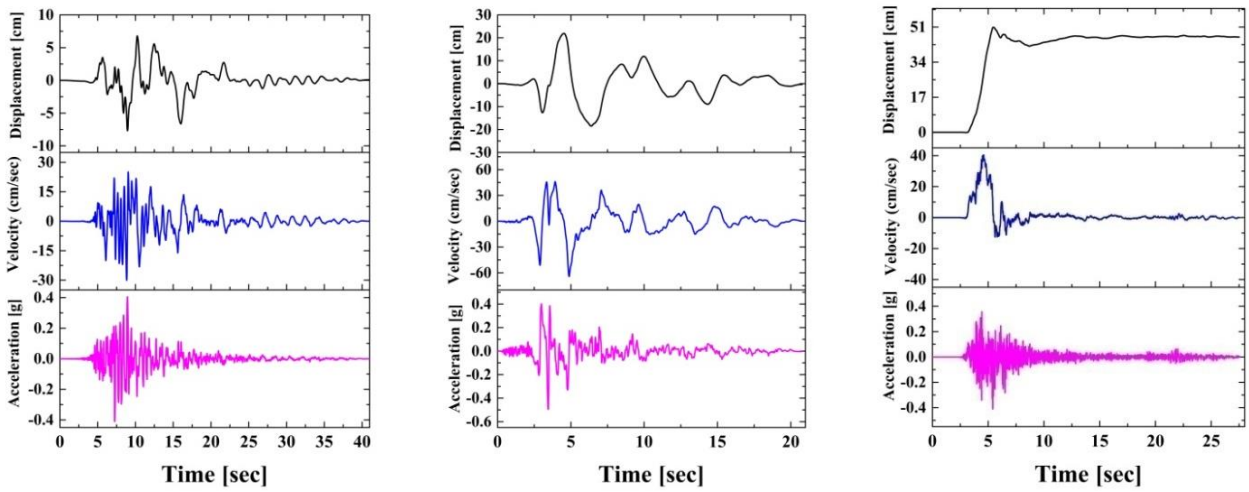

(a) Kobe-Nishi Akashi (FF) earthquake (b) Erzincan (NF-D)earthquake (c) Kocaeli-Sakarya (NF-F) earthquake

Fig. 3 Characteristics of far-field, near-field (with directivity effect, and fling-step effect) earthquakes

Near-Field with Fling-Step Effect (NF-F)			
1	Chi-Chi TCU065 (1999)	7.6-0.76g	EW
2	Chi-Chi TCU072 (1999)	7.6-0.46g	EW
3	Chi-Chi TCU076 (1999)	7.6-0.33g	EW
4	Chi-Chi TCU084 (1999)	7.6-0.98g	EW
5	Kocaeli-Sakarya (1999)	7.4-0.41g	EW

Three types of nonlinearities, viz. the connection nonlinearity in the form of semi-rigid connection, geometric nonlinearity in the form of secondary P-Δ effect, and material nonlinearity. The hysteretic material nonlinearity at the yield sections is considered in the study. The backbone curve for the hysteretic nonlinearity is assumed to be bilinear. Further, it is assumed that concentrated plastic hinges are formed at the yield sections and the bilinear backbone curve at the yield section is defined in terms of moment-rotation plot at the yield section. Note that the value of the '$\boldsymbol{E}$' and '$\boldsymbol{f_y}$' defined in Table 1 are used to calculate the plastic moment capacity of the section and the yield rotation respectively. The default plastic hinge property defined in SAP2000 as per ASCE 41 guidelines is used here to describe the bilinear hysteretic property of the yield section as shown in Fig. 5.

The Indian standard code does not provide the acceptance limits for the plastic hinges for different performance levels. Therefore, the acceptance criteria for plastic hinges are selected from Tables 9-6 of (ASCE-41 (2017)) to estimate the nonlinear seismic response of the SR frames as shown in Fig. 5. The flexural M3 plastic hinges for beams and P-M3 plastic hinges for columns at the ends of flexural members are employed in SAP2000.

Figs. 6 (a) and 6(b) show the capacity curves of one fully rigid and two SR frames, in each for 5-Story and 10-Story building frames. It is observed from the figure that the displacement is increased with reduced base shear in SR frames as compared to fully rigid frames. The normalized lateral force distribution for the fundamental mode adopted for the NSA of 5- and 10-Story frames are shown in Fig. 7.

For validating the NSA predictions, the NTHA is performed at the scaled PGA levels for the specified target displacements. Three different levels of target displacements are selected, covering the elastic-T_{d1} (A to B-), elastic-plastic-T_{d2} (B- to B+), and plastic state-T_{d3} (LS-CP) in the capacity curve as shown in Fig. 6 (Section 3). Note that the points B- and B+ denote points little below and little beyond the point B shown in Fig 5. The zone B- to B+ is the transition zone from the elastic to plastic; the IO state is contained within this zone. The three target displacements correspond to the three damages states, namely, elastic, (no damage, linear variation in the capacity curve), elastic-plastic (slight damage, near or at the onset of yielding or the starting of the inelastic portion of the capacity curve) and plastic (severe damage, at the end segment of the capacity curve, i.e., near the collapse level) are accounted in the comparative numerical study. These three levels of target displacements are categorized into three performance levels, elastic (T_{d1}), elastic-plastic (T_{d2}), and plastic (T_{d3}) as defined in Fig. 6. Note that the target displacements are identified from the visual depiction of the capacity curves. They satisfy the performance levels indicated by the three broad ranges, i.e., A-B, B-IO, and IO-CP of the capacity spectrum method described by ASCE-41 (2017). Further, it may be noted that the target displacements are different for the 5-Story and 10-Story frames.

For the example problem selected, the capacity curves of the two frames are so found that the visual identification of the three levels of target displacements satisfying the aforementioned performance levels led to the differences

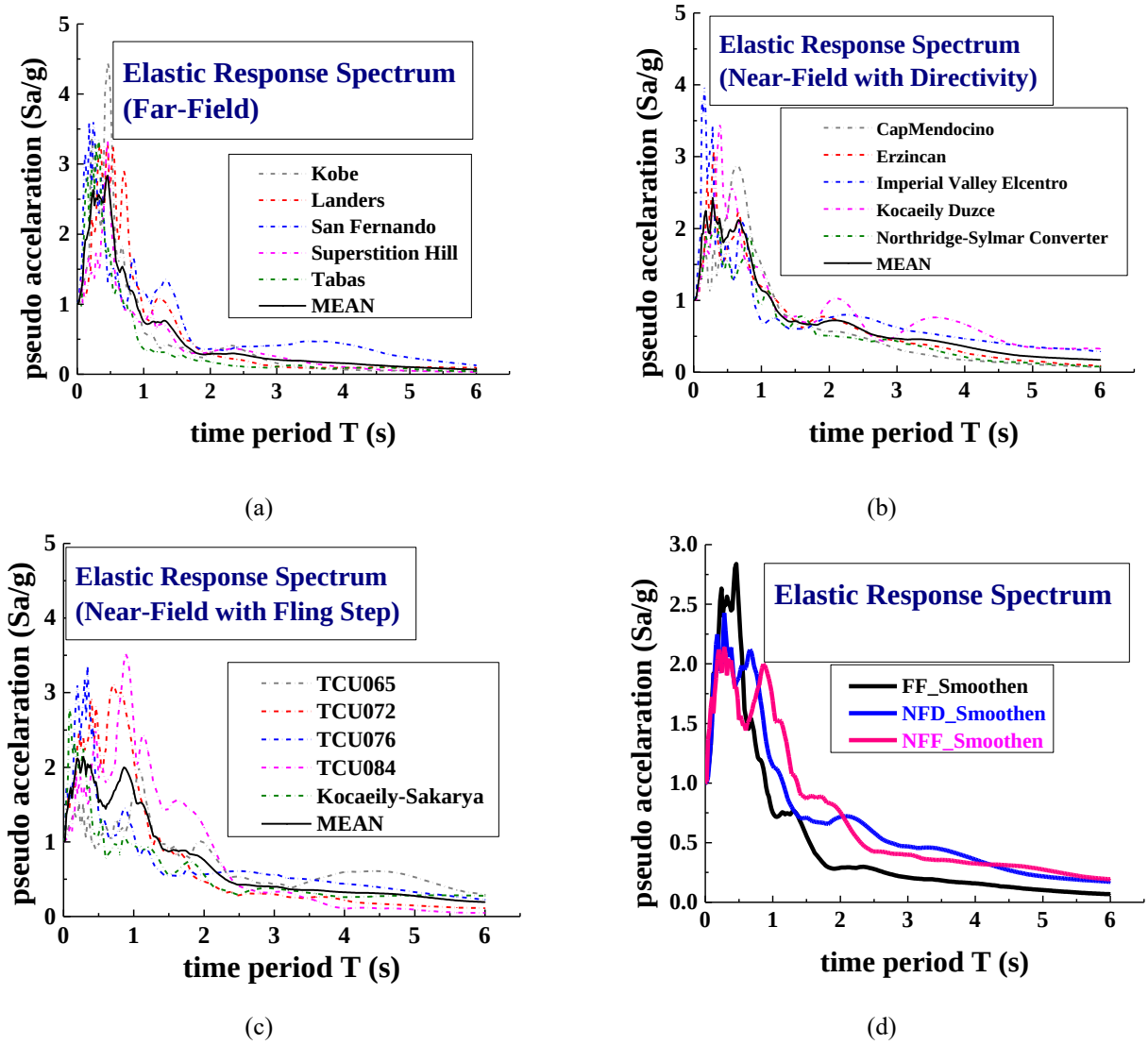

Fig. 4 Elastic responses spectra for different types of earthquakes and mean smoothened elastic response spectra

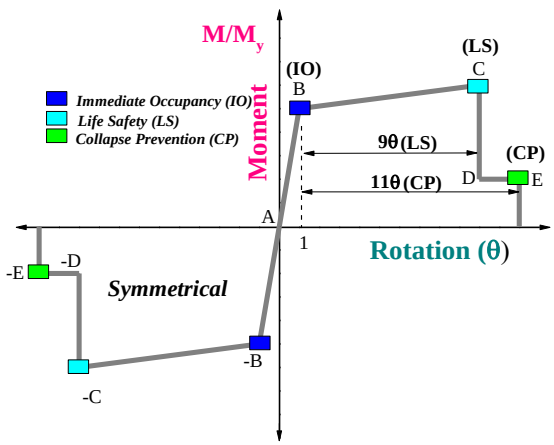

Fig. 5 Backbone curve for the hysteretic behavior of yield section (plastic hinges)

between 'T_ds' of the two frames as (i) very small for T_{d1}, (ii) moderate for T_{d2}, and (iii) small to moderate for T_{d3}. For each target displacement considered in the study, the PGA of each earthquake is scaled such that the peak top-story displacement obtained from the NTHA matches the target displacement as depicted in Fig. 6. The scaled PGA thus obtained are tabulated in Tables 5-6 for the five and ten-story frames.

4. Results and discussion

The responses of rigid and semi-rigid steel frames, predicted by the NSA are evaluated at three levels of target displacements (as discussed before) by comparing those obtained from the NTHA for the scaled earthquakes. The PGAs of the earthquakes are scaled such that the obtained peak top story displacements match with the target displacements. The PGA values of each earthquake forwhich the top story displacements are matched with the target displacements are shown in Tables 5 and 6. The response quantities of interest, namely, the peak top story

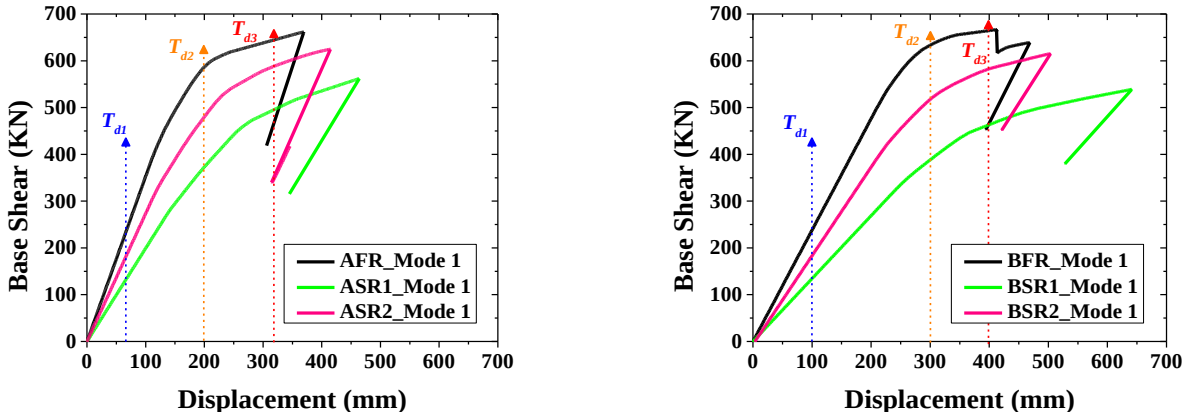

(a) 5-Story Frame (b) 10-Story Frame

Fig. 6 Capacity curves for a fully rigid and semi-rigid steel MR frames

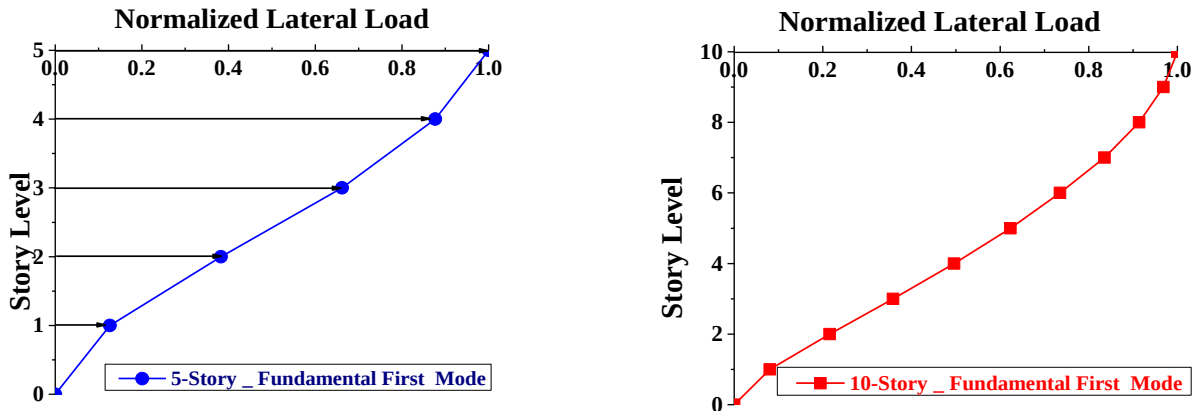

(a) 5-Story Frame (b) 10-Story Frame

Fig. 7 Normalized lateral force pattern for the fundamental mode for nonlinear static analysis

Table 5 Scaled PGA (g) values the corresponding to different levels of target displacements for the 5-Story frame

Earthquake Type	Event Name	AFR (α>20; β=1.5)			ASR1 (α=5; β=1.2)			ASR2 (α=15; β=1.5)		
		T_{d1} 70 (mm)	T_{d2} 200 (mm)	T_{d3} 320 (mm)	T_{d1} 70 (mm)	T_{d2} 200 (mm)	T_{d3} 320 (mm)	T_{d1} 70 (mm)	T_{d2} 200 (mm)	T_{d3} 320 (mm)
Far-field (FF)	Kobe	0.35	1.051	1.732	0.2785	0.855	1.34	0.29	0.851	1.643
	Landers	0.251	0.715	1.0757	0.108	0.308	0.4899	0.182	0.575	0.805
	Sanfernando	0.1705	0.605	1.117	0.0875	0.2712	0.543	0.1614	0.585	0.865
	Superstition	0.252	0.895	1.902	0.16	0.477	0.9767	0.1851	0.786	1.435
	Tabas	0.57	1.693	2.96	0.4323	1.278	2.26	0.514	1.61	2.968
Near-field with directivity (NF-D)	Erzincan	0.1649	0.479	0.746	0.1374	0.3888	0.6078	0.1532	0.4316	0.6635
	Imperial Valley	0.3015	0.8965	1.268	0.18	0.524	0.8636	0.22	0.631	1.074
	Northridge	0.1754	0.4805	0.835	0.1929	0.5655	0.922	0.1614	0.481	1.112
	Kocaeily Duzce	0.1422	0.435	0.87	0.162	0.4557	0.692	0.148	0.5144	0.7617
	Cap Mendocino	0.14	0.412	0.888	0.144	0.4115	0.637	0.1383	0.4542	0.752
Near-field with fling step effects (NF-F)	TCU065	0.102	0.373	0.709	0.111	0.319	0.663	0.1015	0.3306	0.6715
	TCU072	0.1055	0.3261	0.8	0.11	0.3174	0.615	0.1108	0.385	0.818
	TCU076	0.208	0.622	1.291	0.1107	0.3155	0.5915	0.1705	0.4929	1.1098
	TCU084	0.1015	0.3015	0.581	0.0723	0.218	0.4005	0.0676	0.2345	0.459
	Kocaeily - Sakarya	0.214	0.773	1.14	0.1484	0.421	0.65	0.1695	0.4775	0.7651

Table 6 Scaled PGA (g) values the corresponding to different levels of target displacements for the 10-Story frame

Earthquake Type	Event Name	BFR (α>20; β=1.5)			BSR1 (α=5; β=1.2)			BSR2 (α=15; β=1.5)		
		T_{d1}	T_{d2}	T_{d3}	T_{d1}	T_{d2}	T_{d3}	T_{d1}	T_{d2}	T_{d3}
		100 mm	300 mm	400 mm	100 mm	300 mm	400 mm	100 mm	300 mm	400 mm
FF	Kobe	0.362	1.035	1.3263	0.1481	0.445	0.6119	0.2075	0.6537	1.1498
	Landers	0.2685	0.803	1.1455	0.332	0.9723	1.263	0.2558	0.7806	1.1187
	Sanfernando	0.235	0.705	0.9132	0.135	0.4212	0.6041	0.1853	0.555	0.7491
	Superstition	0.2915	1.151	1.522	0.1415	0.4667	0.7389	0.217	0.7776	1.0287
	Tabas	0.51	1.525	2.137	0.3998	1.1995	1.6955	0.4168	1.315	1.8781
NF-D	Erzincan	0.124	0.4678	0.835	0.0924	0.2808	0.3882	0.1038	0.3382	0.4978
	Imperial Valley	0.1182	0.3582	0.5571	0.065	0.1949	0.323	0.0872	0.2613	0.4305
	Northridge	0.1719	0.5994	0.8004	0.1042	0.3127	0.4801	0.1326	0.4238	0.7148
	Kocaeily-Duzce	0.116	0.4	0.5351	0.0744	0.2225	0.3077	0.0689	0.2105	0.3598
	Cap Mendocino	0.1418	0.44	0.588	0.0935	0.2797	0.4905	0.1108	0.3648	0.5334
NF-F	TCU065	0.095	0.3037	0.5448	0.091	0.2784	0.4335	0.0805	0.252	0.4815
	TCU072	0.1565	0.492	0.729	0.1735	0.5035	0.7435	0.1577	0.4671	0.6395
	TCU076	0.1627	0.488	0.6202	0.0819	0.2471	0.3285	0.1241	0.3715	0.4905
	TCU084	0.0625	0.2005	0.478	0.1182	0.405	0.5917	0.0661	0.2178	0.5075
	Kocaeily -Sakarya	0.1262	0.4326	0.7806	0.1612	0.481	0.6514	0.1527	0.4641	0.7448

displacement (PSD),), maximum inter-story drift ratio (IDR_{max}), peak-base shear (BS_{peak}), total number of plastic hinges, and SRSS of maximum plastic hinge rotations are determined from the NTHA carried out for each scaled earthquake with the PGA as shown in Tables 5 and 6. The responses thus obtained are compared with those of the NSA for each level of the target displacement. The comparison is carried out in the form of the root mean square error (E_{rms}) in responses, as explained in Eqs. (2) and (3).

$$\boldsymbol{E_{rms,i}} = \sqrt{\frac{1}{5}\sum_{i=1}^{5}\left(\boldsymbol{error_{ijt}}\right)^2} \tag{2}$$

where, 'i' is the earthquake number, here i= 1 to 5; j= earthquake type (FF, NF-D or NF-F); and t= target displacement (T_{d1}, T_{d2} or T_{d3}); and

$$\boldsymbol{error_{ijt}} = \frac{\left((\boldsymbol{NSA})_t - (\boldsymbol{NTHA})_{ijt}\right)}{(\boldsymbol{NTHA})_{ijt}} \tag{3}$$

where $(NSA)_t$ is the maximum absolute value of the response obtained by the NSA for the target displacement 't' and $(NTHA)_{ijt}$ indicates the response at the same target displacement level 't' for the ith number and j^{th} type of the earthquake.

For the comparison, E_{rms} values are determined for the PSD, IDR_{max}, BS_{peak}, total number of plastic hinges, and SRSS of maximum plastic hinge rotations. E_{rms} is taken as an assessment indicator which shows how good are the response predictions by the NSA at different levels of target displacement when compared with the responses of the NTHA_In the following sections, this comparison is made using E_{rms} for each response quantities of interest._Further, the energy dissipation in connections and plastic hinges are evaluated for different degrees of semi-rigidity (D_{SR}) and types of earthquakes for each target level from the NTHA. They are compared in order to show how the type of earthquake influence the total inelastic excursion of the frames. The comparison between the responses obtained by the NSA and NTHA is fair so long as the contributions of the higher modes (than the fundamental mode) are not significant in the responses obtained by the NTHA. However, for flexible structures like SR frames, the possibility of the contributions of the higher modes in the responses (in the linear range) might be more in the NTHA making the above comparison questionable. As the structure undergoes inelastic excursion, contributions of the higher modes in the responses become a complex phenomena and are invariably present in all types of structures, flexible or rigid. Despite this fact, the comparison of responses between the NSA and NTHA has been a standard practice in the literature on this subject. In the present study, the comparisons are made consistent with the standard practice in the literature (inspite of the knowledge of above facts).

4.1 Comparison of peak top-story displacement

The E_{rms} error for the peak top-story displacement (PSD) along the story height is shown for the three types of earthquakes and three degrees of joint stiffness or semi-rigidity (one fully rigid and two semi-rigid) in Figs. 8 and 9 for the 5- and 10-Story frames. It is observed from Fig. 8 that for the 5-Story frame, the error increases with the decrease in the story level; the bottom story (or the second story) exhibits the maximum error, whereas the upper stories show very less errors. The trend remains the same

irrespective of the type of earthquake and the degree of the semi-rigidity. In general, it is seen that the error is less for the near field, NF-F earthquake. Except for the far-field earthquake at the target level T_{d3} (plastic state), all errors remain within 15 to 20%. So far as the effect of the degree of semi-rigidity on E_{rms} is concerned, no definite pattern is observed.

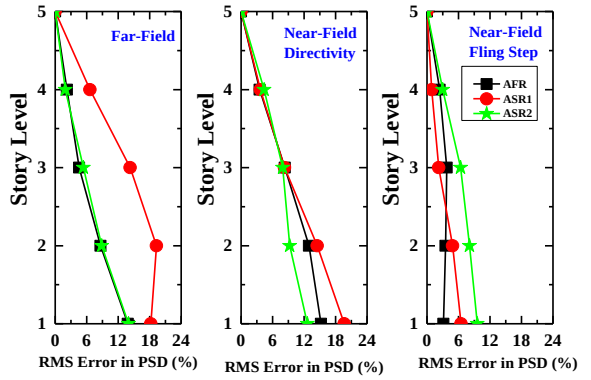

(a) 5-Story T_{d1} =70 mm

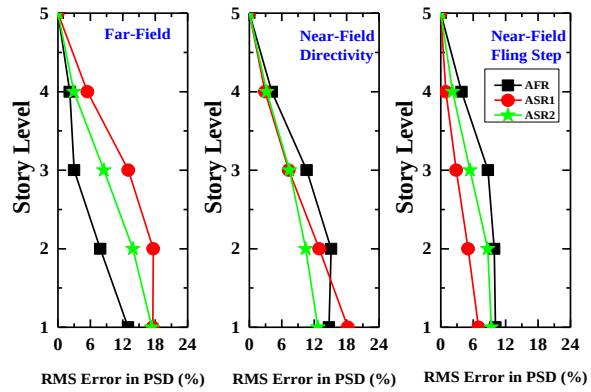

(b) 5-Story T_{d2} = 200 mm

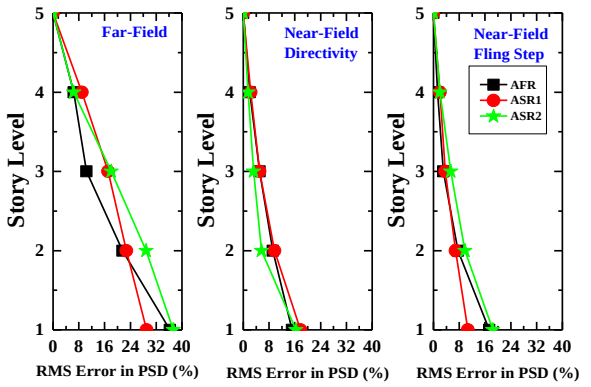

(c) 5-Story T_{d3} =320 mm

Fig. 8 Variation of E_{rms} values along the story height for the PSD at different levels of target displacements (5-Story frame)

A similar trend of results for the 10-Story frame is observed with two differences (i) the maximum error goes up to 25-30% and (ii) the maximum error in certain cases, is observed at the fourth story level, rather than the first story level.

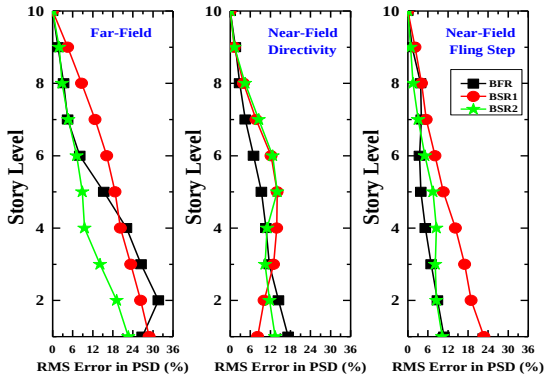

(a) 10-Story T_{d1} = 100 mm

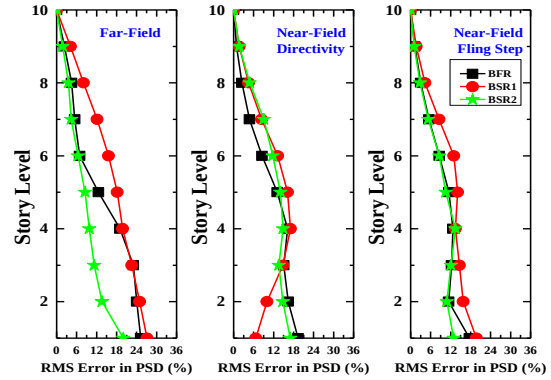

(b) 10-Story T_{d2} = 300 mm

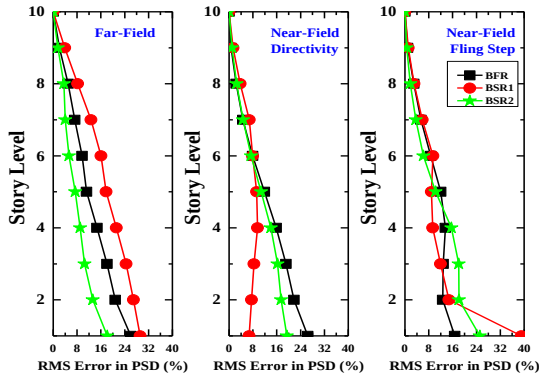

(c) 10-Story T_{d3} = 400 mm

Fig. 9 Variation of E_{rms} values along the story height for the PSD at different levels of target displacements (10-Story frame)

4.2 Comparison of the maximum inter-story drift (IDR_{max}) ratio

The variation of E_{rms} error in maximum inter-story drift ratio (IDR_{max}) along with the story height for the five and ten-story frames at three target displacements obtained for different types of earthquakes are shown in Figs. 10 and 11.

Unlike the variation along with the height for the peak top-story displacement, considerable error in IDR_{max} is exhibited at the top story level and upper stories. This is the case because the maximum top story displacement (at the target displacement) obtained from the NTHA is matched with the NSA. As a consequence, no error is observed for the case of peak top story displacement. The effect of this

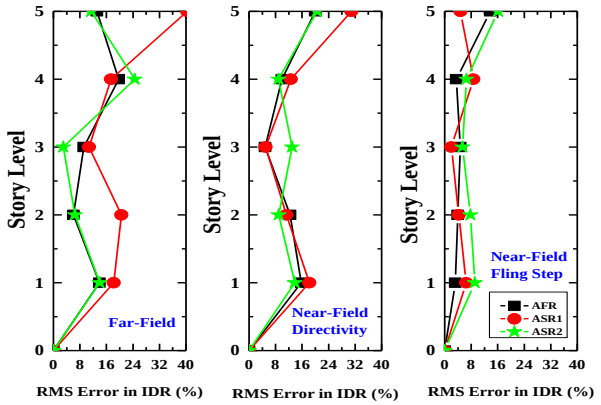

(a) 5-Story T_{d1} =70 mm

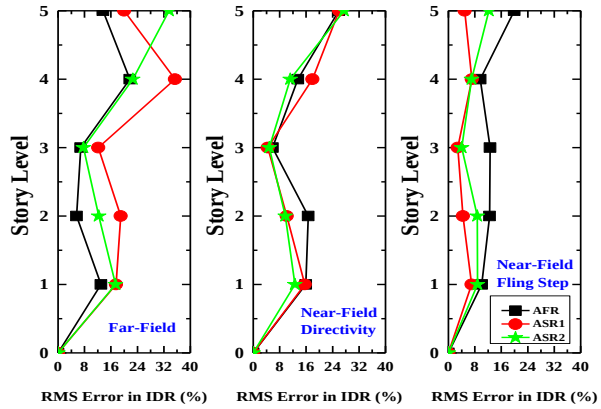

(b) 5-Story T_{d2} = 200 mm

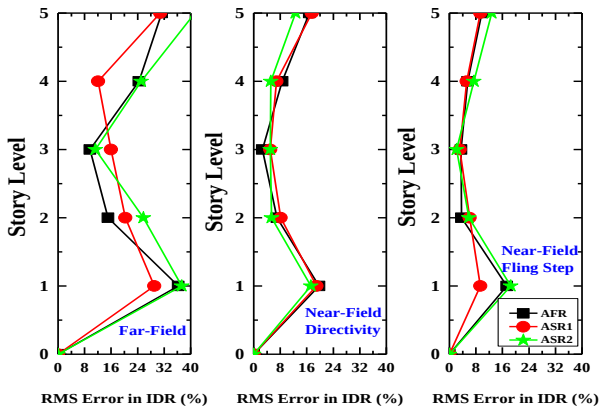

(c) 5-Story T_{d3} =320 mm

Fig. 10 Variation of E_{rms} values along the story height for the IDR_{max} at different levels of target displacements (5-Story frame)

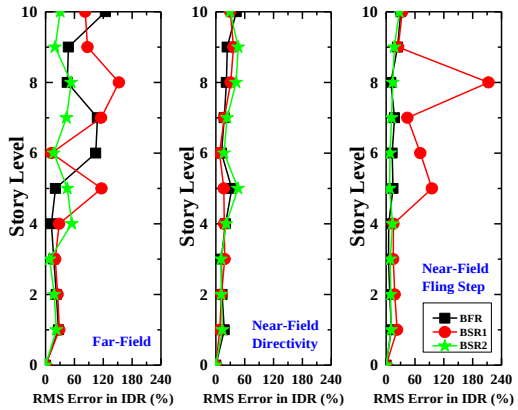

(a) 10-Story T_{d1} =100 mm

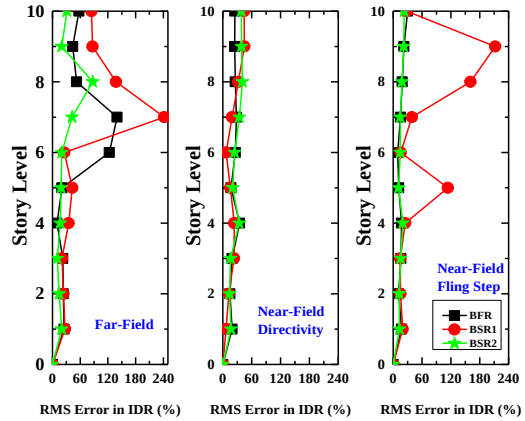

(b) 10-Story T_{d2} = 300 mm

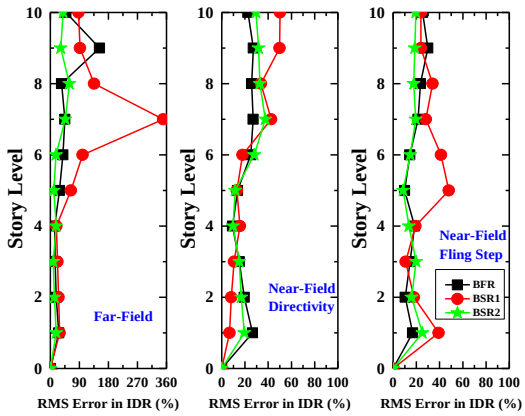

(c) 10-Story T_{d3} =400 mm

Fig. 11 Variation of E_{rms} values along the story height for the IDR_{max} at different levels of target displacements (10-Story frame)

displacement matching continues at the upper floor levels and decreases considerably at the lower story level, resulting in an increased error in the peak floor displacement at the bottom story level.

Since the PGAs of the earthquakes are not scaled based on the drift matching, a substantial difference in IDR_{max} obtained by the two analyses. From Figs. 10 and 11, it is observed that no fixed pattern of variation of the E_{rms} in IDR_{max} is observed along the height. However, in general, it is observed that E_{rms} is less in the middle stories of the frames. Further, E_{rms} is generally less for the near-field earthquakes as compared to the far-field earthquakes and the maximum value of E_{rms} remains in the range of 16-32% for the five-story frame.

For the 10-Story frame, the maximum value of E_{rms} is significantly large in the range of 50-300%. Further, it is observed from the figures that no consistent relationship exists between the degree of semi-rigidity with the E_{rms}.

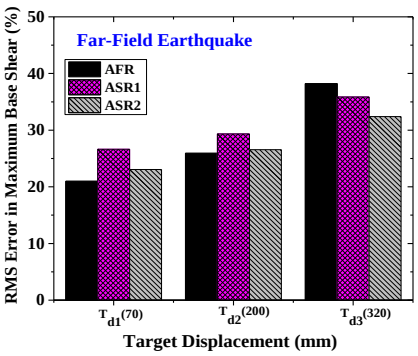

(a)

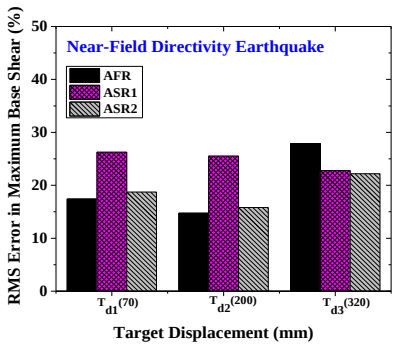

(b)

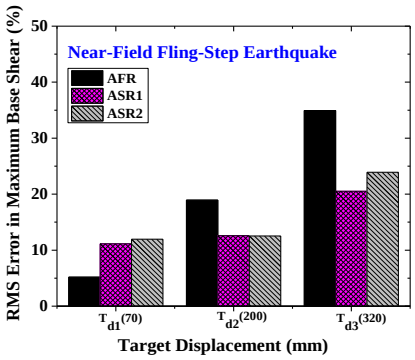

(c)

Fig. 12 E_{rms} values for the base shear at different levels of target displacements (5-Story frame)

4.3 Assessment of the peak base shear (BS_{peak})

E_{rms} in the peak base shear (BS_{peak}) for the five- and ten-story frames at the three levels of target displacements for different types of earthquakes are shown in Figs. 12 and 13.

It is observed from the figures that the E_{rms}, in general, is more at the target displacement T_{d3} as compared to the T_{d2} and T_{d1}. The maximum E_{rms} ranges between 20-40% for most of the cases. Here again, no consistent relationship between the degree of semi-rigidity and E_{rms} is noticed.

4.4 Comparison of plastic hinges and SRSS of hinge rotations

The number of plastic hinges formed in the NTHA and NSA, and the percentage difference between the two is shown in Table 7.

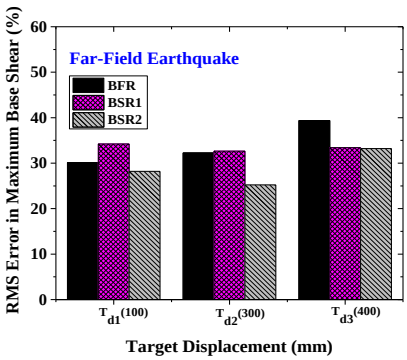

(a)

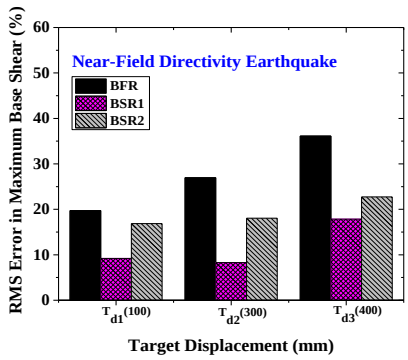

(b)

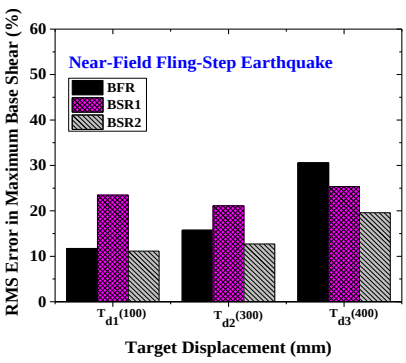

(c)

Fig. 13 E_{rms} values for the base shear at different levels of target displacements (10-Story frame)

Table 7 Total number of plastic hinges at different levels of target displacements

Frame ID	Far-Field			Near-Field with Directivity			Near-Field with Fling Step		
	Mean NTHA	NSA	% Difference	Mean NTHA	NSA	% Difference	Mean NTHA	NSA	% Difference
5-Story Frames (Target Displacement T_{d3} =320 mm)									
AFR	45	25	44.44	36	25	30.56	36	25	30.56
ASR2	29	10	65.52	17	10	41.18	18	10	44.44
ASR1	6	4	33.33	5	4	20.00	4	4	0.00
10-Story Frames (Target Displacement T_{d3} =400 mm)									
BFR	68	34	50.00	51	34	33.33	49	34	30.61
BSR2	26	4	84.62	12	4	66.67	6	4	33.33
BSR1	5	3	40.00	3	3	0.00	3	3	0.00
5-Story Frames (Target Displacement T_{d2} =200 mm)									
AFR	29	17	41.38	22	17	22.73	25	17	32.00
ASR2	6	0	100.00	2	0	100.00	1	0	100.00
ASR1	1	0	100.00	1	0	100.00	0	0	0.00
10-Story Frames (Target Displacement T_{d2} =300 mm)									
BFR	50	24	52.00	40	24	40.00	35	24	31.43
BSR2	6	3	50.00	3	3	0.00	3	3	0.00
BSR1	4	0	100.00	0	0	0	1	0	100.00

Table 8 SRSS of maximum plastic hinge rotations (SRSS) in radian at different levels of target displacements

Frame ID	Far-Field			Near-Field with Directivity			Near-Field with Fling Step		
	Mean NTHA	NSA	% Difference	Mean NTHA	NSA	% Difference	Mean NTHA	NSA	% Difference
5-Story Frames (Target Displacement T_{d3} =320 mm)									
AFR	0.0718	0.0595	17.17	0.0677	0.0595	12.14	0.0681	0.0595	12.57
ASR2	0.0101	0.0138	-36.96	0.0082	0.0138	-67.63	0.0085	0.0138	-61.58
ASR1	0.0036	0.0080	-119.94	0.0046	0.0080	-74.78	0.0049	0.0080	-62.67
10-Story Frames (Target Displacement T_{d3} =400 mm)									
BFR	0.0451	0.0426	5.39	0.0435	0.0426	1.95	0.0420	0.0426	-1.59
BSR2	0.0062	0.0079	-26.85	0.0060	0.0079	-31.51	0.0034	0.0079	-130.19
BSR1	0.0046	0.0023	50.88	0.0017	0.0023	-35.96	0.0023	0.0023	0.67
5-Story Frames (Target Displacement T_{d2} =200 mm)									
AFR	0.0332	0.0258	22.28	0.0244	0.0258	-5.69	0.0280	0.0258	7.69
ASR2	0.0008	0.0000	100.00	0.0003	0.0000	100.00	0.0001	0.0000	100.00
ASR1	0.0004	0.0000	100.00	0.0002	0.0000	100.00	0.0000	0.0000	0.00
10-Story Frames (Target Displacement T_{d2} =300 mm)									
BFR	0.0209	0.0181	13.15	0.0174	0.0181	-4.32	0.0141	0.0181	-29.04
BSR2	0.0011	0.0005	54.74	0.0013	0.0005	62.24	0.0001	0.0005	-290.70
BSR1	0.0011	0.0000	100.00	0.0000	0.0000	0.00	0.0001	0.0000	100.00

Note that the number of plastic hinges shown for the NTHA is the mean of the number of plastic hinges formed for each earthquake in the ensemble of earthquakes of a particular type. It is seen from the table that the number of plastic hinges formed for the rigid frame is much more as compared to SR frames. The difference in the number of plastic hinges formed between the NSA and NTHA is large for the rigid frame. The difference is maximum at the target level T_{d3} and more for far-field earthquakes (as the PGA values for the FF earthquakes are higher, as shown in Tables 5 and 6). The maximum difference in most of the cases is the order of 40-60%, the NTHA providing more number of plastic hinges.

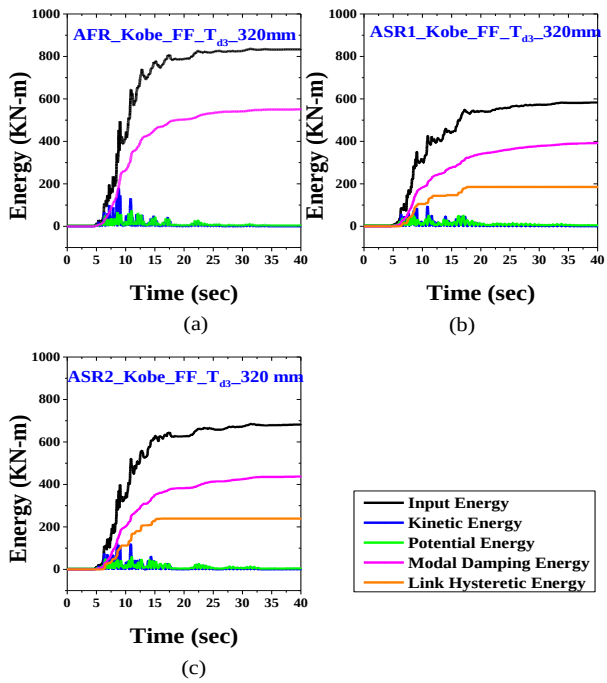

Fig. 14 Energy dissipation in the rigid and semi-rigid frames (a-c) under far-field earthquakes

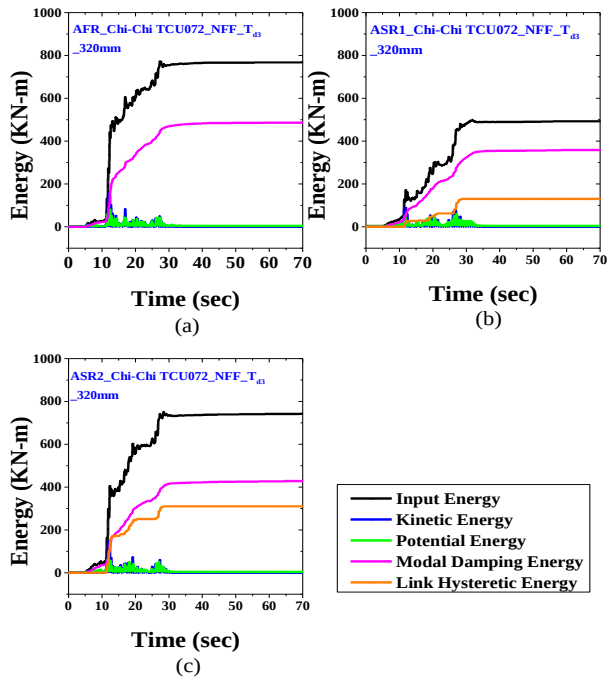

Fig. 15 Energy dissipation in the rigid and semi-rigid frames (a-c) under near-field earthquakes

From the same table, it is seen that although the percentage difference between the number of plastic hinges formed in the NTHA and NSA is large, this difference is not of much practical consequence as the number of plastic hinges formed in both analyses is very less. Thus, for all practical purposes, the NSA may be able to predict the number of plastic hinges formed in SR frames fairly well.

The formation of the less number of plastic hinges in SR frames is expected as it attracts less seismic energy as compared to the rigid frame as shown in Figs. 14 and 15. The input energy in the rigid frame is higher as compared to that in the SR frame. Further, it may be noted that most of the energy attracted by the semi-rigid frames are dissipated in the plastic-link elements, resulting in less seismic energy left for the formation of plastic hinges in semi-rigid frame.

Table 8 shows the SRSS of maximum plastic hinge rotations in both analyses. In the case of the NTHA, the values of maximum plastic hinge rotation are the mean of the SRSS of plastic hinge rotations formed for the earthquakes in the ensemble of a particular type of earthquake. It is seen from the table that the maximum plastic hinge rotations are much higher in the NSA. The maximum difference in most cases is of the order of 100-130%. Note that, in the case of SR frames, although the number of plastic hinges are less in both analyses, the difference in the plastic hinge rotations is quite significant between the two analyses. Thus, in terms of predicting the maximum plastic hinge rotation, NSA is not a good predictor. Note that, the SRSS of the maximum plastic hinge rotation out of all the cases considered does not exceed the permissible plastic hinge rotation as prescribed in the AISC 360-16. Thus, the code requirements in respect to damage limitations in terms of plastic hinge rotation is met in the worst scenario considered here.

5. Conclusions

Predictions of the NSA with those of the NTHA are compared for semi-rigid frames at three levels of target displacements which lie in the range of elastic, elastic-plastic, and plastic state. The NTHA is performed for scaled PGA levels for which the peak top story displacement of the frames matches with the selected target displacements fixed on the capacity curves. The comparison is intended to validate predictions of the responses by the NSA. Three different types of earthquakes are considered, namely, the far-field, near-field with directivity, and fling step effects. In each type of earthquake, an ensemble of five real earthquake records is selected from the PEER ground motion database. Three degrees of semi-rigidity or joint stiffness (one fully rigid and two semi-rigid) are used to evaluate the effect of the degree of semi-rigidity on the response evaluation. The response quantities of interest include the peak story displacement, maximum base shear, maximum inter-story drift ratio, number of total plastic hinges, and SRSS of maximum plastic hinge rotations. The results of the numerical study lead to the following conclusions.

(1) Fairly good predictions of the peak story displacements are met by the NSA at all the three target displacements for different types of earthquakes with the E_{rms} (Eqs. (2) and (3)) value remaining in within 15-20% for the 5-story frame and 25-30% for the 10-Story frame; the degree of joint stiffness or semi-rigidity does not have a correlation with the E_{rms}.

(2) For the five-story frame, the predictions of the maximum inter-story drift by the NSA compare fairly well with the E_{rms} value lying between 16-32%; for the ten-story frame, the predictions are extremely poor showing E_{rms} value of the order of 300%; further, it is noted that the E_{rms} value is quite significant for the maximum inter-story drift at the top story level where the target displacements are matched between the NTHA and NSA.

(3) The base shear predictions by the NSA are fairly well in certain cases with E_{rms} values lying between 20-40%.

(4) The NTHA provides more number of plastic hinges, about 40-60% more than those provided by the NSA for the rigid frames; for the semi-rigid frames, the number of plastic hinges formed are drastically reduced in both NSA and NTHA. The percentage difference between the two numbers is not of much concern as the number of plastic hinges formed are themselves very less. Thus, the NSA can be performed to get an estimate of the number of plastic hinges formed in the semi-rigid frame at the considered target displacements.

(5) Even though the predictions of the number of plastic hinges by the NSA are reasonably well for the semi-rigid frames, the SRSS of maximum plastic hinge rotation is found to be much higher for the NSA as compared to the NTHA.

Acknowledgments

The authors thankfully acknowledge the Department of Civil Engineering, MNIT Jaipur, and Quality Improvement Program (QIP) center, MNIT Jaipur, India, for providing research facilities. Sincere thanks are also to All India Council for Technical Education (AICTE), New Delhi, India for providing financial support in the form of research scholarship. Authors also wish to express gratitude to Government Engineering College, Palanpur, Gujarat state, India, and Commissionerate of Technical Education, Gujarat state, India for financial support to conduct this study.

References

Abdollahzadeh, G., Faghihmaleki, H. and Esmaili, H. (2016), "Comparing Hysteretic Energy and inter-story drift in steel frames with V-shaped brace under near and far fault earthquakes", *Alexandria Eng. J.*, **57**(1), 301-308. http://dx.doi.org/10.1016/j.aej.2016.09.015.

AISC-360, B. (2016), *AISC 360-16, Specification for Structural Steel Buildings*,

Aksoylar, N.D., Elnashai, A.S. and Mahmoud, H. (2011), "The design and seismic performance of low-rise long-span frames with semi-rigid connections", *J. Constr. Steel Res.*, **67**(1), 114-126. https://doi.org/10.1016/j.jcsr.2010.07.001.

Al-Bermani, F., Li, B., Zhu, K. and Kitipornchai, S. (1994), "Cyclic and seismic response of flexibly jointed frames", *Eng. Struct.*, **16**(4), 249-255. https://doi.org/10.1016/0141-0296(94)90064-7.

ANSI/AISC-341 (2016), *341 Seismic provisions for structural steel buildings*,

Antoniou, S. and Pinho, R. (2004), "Development and verification of a displacement-based adaptive pushover procedure", *J. Earthq. Eng.*, **8**(05), 643-661. http://dx.doi.org/10.1080/13632460409350504.

ASCE-41 (2017), *ASCE 41-17: Seismic Evaluation and Retrofit Rehabilitation of Existing Buildings*,

ATC-40 (1996), *Seismic evaluation and retrofit of concrete buildings- Volume I*, Applied Technology Council, California Seismic Safety Commission, Redwood City, California, 94065.

Awkar, J. and Lui, E.M. (1999), "Seismic analysis and response of multistory semirigid frames", *Eng. Struct.*, **21**(5), 425-441. https://doi.org/10.1016/S0141-0296(97)00210-1.

Bayat, M. and Zahrai, S.M. (2017), "Seismic performance of mid-rise steel frames with semi-rigid connections having different moment capacity", *Steel Compos. Struct.*, **25**(1), 1-17. https://doi.org/10.12989/scs.2017.25.1.000.

Bhandari, M., Bharti, S., Shrimali, M. and Datta, T. (2018), "Assessment of proposed lateral load patterns in pushover analysis for base-isolated frames", *Eng. Struct.*, **175** 531-548. https://doi.org/10.1016/j.engstruct.2018.08.080.

Bracci, J.M., Kunnath, S.K. and Reinhorn, A.M. (1997), "Seismic performance and retrofit evaluation of reinforced concrete structures", *J. Struct. Eng.*, **123**(1), 3-10. https://doi.org/10.1061/(ASCE)0733-9445(1997)123:1(3).

Brunesi, E., Nascimbene, R. and Rassati, G. (2015), "Seismic response of MRFs with partially-restrained bolted beam-to-column connections through FE analyses", *J. Constr. Steel Res.*, **107** 37-49. http://dx.doi.org/10.1061/(ASCE)CF.1943-5509.0000628.

Chan, S. and Chui, P. (2000), *Nonlinear static and cyclic analysis of steel frames with semi-rigid connections*, Elsevier

Chopra, A.K. and Goel, R.K. (2002), "A modal pushover analysis procedure for estimating seismic demands for buildings", *Earthq. Eng. Struct. D.*, **31**(3), 561-582. https://doi.org/10.1002/eqe.144.

Diaferio, M. (2018), "Performance of seismic shear panels under near-field motions", *Int. J. Eng. Technol.*, **7**(2), 196-200. https://www.sciencepubco.com/index.php/ijet/article/view/11915/4685

Diaferio, M. and Foti, D. (2016), "Mechanical behavior of buildings subjected to impulsive motions", *Bull. Earthq. Eng.*, **14**(3), 849-862. https://doi.org/10.14419/ijet.v7i2.23.11915.

Elnashai, A. and Elghazouli, A. (1994), "Seismic behaviour of semi-rigid steel frames", *J. Constr. Steel Res.*, **29**(1-3), 149-174. https://doi.org/10.1016/0143-974X(94)90060-4.

Erduran, E. (2008), "Assessment of current nonlinear static procedures on the estimation of torsional effects in low-rise frame buildings", *Eng. Struct.*, **30**(9), 2548-2558. https://doi.org/10.1016/j.engstruct.2008.02.008.

Eurocode 3, B.S. (2006), "Eurocode 3—Design of steel structures—", *BS EN 1993-1*. **1** 2005.

Faridmehr, I., Tahir, M.M. and Lahmer, T. (2016), "Classification system for semi-rigid beam-to-column connections", *Latin Am. J. Solids \Struct.*, **13**(11), 2152-2175. http://dx.doi.org/10.1590/1679-78252595.

Faridmehr, I., Tahir, M.M., Lahmer, T. and Osman, M.H. (2017), "Seismic Performance of Steel Frames with Semirigid Connections", *J. Eng.*, **2017**. https://doi.org/10.1155/2017/5284247.

Feizi, M.G., Mojtahedi, A. and Nourani, V. (2015), "Effect of semi-rigid connections in improvement of seismic performance of steel moment-resisting frames", *Steel Compos. Struct.*, **19**(2), 467-484. http://dx.doi.org/10.12989/scs.2015.19.2.467

FEMA-355D (2001), *State of the art report on connection performance*,

FEMA-440 (2005), "440, Improvement of nonlinear static seismic analysis procedures", *FEMA-440, Redwood City*. **7**(9), 11.

FEMA-P695 (2009), *Quantification of building seismic performance factors*, Federal Emergency Management Agency

Foti, D. (2014), "On the seismic response of protected and unprotected middle-rise steel frames in far-field and near-field areas", *Shock Vib*., **2014**. http://dx.doi.org/10.1155/2014/393870.

Foti, D. (2014), "Response of frames seismically protected with passive systems in near-field areas", *Int. J. Struct. Eng*., **5**(4), 326-345. http://www.inderscience.com/info/ingeneral/forthcoming.php?jcode=ijstructe

Foti, D. (2015), "Local ground effects in near-field and far-field areas on seismically protected buildings", *Soil Dynam. Earthq. Eng*., **74** 14-24. http://dx.doi.org/10.1016/j.soildyn.2015.03.005

Hasan, R., Xu, L. and Grierson, D. (2002), "Push-over analysis for performance-based seismic design", *Comput. Struct*., **80**(31), 2483-2493. https://doi.org/10.1016/S0045-7949(02)00212-2.

Hsieh, S.H. and Deierlein, G. (1991), "Nonlinear analysis of three-dimensional steel frames with semi-rigid connections", *Comput. Struct*., **41**(5), 995-1009. https://doi.org/10.1016/0045-7949(91)90293-U.

IS-800 (2007), *General Construction in Steel-Code of Practice (*Third Revision) Bureau of Indian Standards, New Delhi.

IS-875 (1987), Part 1: DEAD LOADS — UNIT WEIGHTS OF BUILDING MATERIALS AND STORED MATERIALS, Bureau of Indian Standards, New Delhi.

IS-1893 (2016), Criteria for earthquake resistant design of structures, Part 1 General Provisions and Buildings (Sixth Revision), Bureau of Indian Standards, New Delhi.

Kalkan, E. and Kunnath, S.K. (2006), "Adaptive modal combination procedure for nonlinear static analysis of building structures", *J. Struct. Eng. - ASCE*. **132**(11), 1721-1731. https://doi.org/10.1061/(ASCE)0733-9445(2006)132:11(1721).

Kalkan, E. and Kunnath, S.K. (2006), "Effects of fling step and forward directivity on seismic response of buildings", *Earthq. Spectra*, **22**(2), 367-390. https://doi.org/10.1193/1.2192560.

Kalkan, E. and Kunnath, S.K. (2007), "Assessment of current nonlinear static procedures for seismic evaluation of buildings", *Eng. Struct*., **29**(3), 305-316. https://doi.org/10.1016/j.jcsr.2010.03.001.

Krolo, P., Čaušević, M. and Bulić, M. (2015), "Nonlinear seismic analysis of steel frame with semi-rigid joints", *Gradjevinar*. **67**(6), 573-583. https://doi.org/10.14256/JCE.1139.2014

Kunnath, S.K. and Kalkan, E. (2004), "Evaluation of seismic deformation demands using nonlinear procedures in multistory steel and concrete moment frames", *ISET J. Earthq. Technol*., **41**(1), 159-181. http://home.iitk.ac.in/~vinaykg/Iset445

Lemonis, M. (2018), "Steel moment resisting frames with both joint and beam dissipation zones", *J. Constr. Steel Res.*. **147** 224-235. https://doi.org/10.1016/j.jcsr.2018.03.020.

Liu, Y., Xu, L. and Grierson, D.E. (2008), "Compound-element modeling accounting for semi-rigid connections and member plasticity", *Eng. Struct*., **30**(5), 1292-1307. https://doi.org/10.1016/j.engstruct.2007.07.026.

Lui, E. and Lopes, A. (1997), "Dynamic analysis and response of semirigid frames", *Eng. Struct.,* **19**(8), 644-654. https://doi.org/10.1016/S0141-0296(96)00143-5.

Mwafy, A. and Elnashai, A. (2001), "Static pushover versus dynamic collapse analysis of RC buildings", *Eng. Struct*., **23**(5), 407-424. https://doi.org/10.1016/S0141-0296(00)00068-7.

Nader, M. and Astaneh, A. (1991), "Dynamic behavior of flexible, semirigid and rigid steel frames", *J. Constr. Steel Res*., **18**(3), 179-192. https://doi.org/10.1016/0143-974X(91)90024-U.

Pirmoz, A. and Liu, M.M. (2017), "Direct displacement-based seismic design of semi-rigid steel frames", *J. Constr. Steel Res.*, **128** 201-209. https://doi.org/10.1016/j.jcsr.2016.08.015.

Poursha, M. and Amini, M.A. (2015), "A single-run multi-mode pushover analysis to account for the effect of higher modes in estimating the seismic demands of tall buildings", *Bull Earthq. Eng*., https://doi.org/10.1007/s10518-014-9721-y.

Reyes, J.C. and Kalkan, E. (2012), "How many records should be used in an ASCE/SEI-7 ground motion scaling procedure?", *Earthq. Spectra*, **28**(3), 1223-1242. https://doi.org/10.1193/1.4000066.

Roldán, R., Sullivan, T. and Della Corte, G. (2016), "Displacement-based design of steel moment resisting frames with partially-restrained beam-to-column joints", *Bull. Earthq. Eng.*, **14**(4), 1017-1046. https://doi.org/10.1007/s10518-016-9879-6.

SAP2000v21 (2019), "Integrated Software for Structural Analysis and Design", *Computers and structures Inc, Berkeley, CA, USA*.

Sharma, V., Shrimali, M., Bharti, S. and Datta, T. (2018). "Behavior of semi-rigid frames under seismic excitations", *Proceedings of the 16th Symposium on Earthquake Engineering*, Indian Institute of Technology, Roorkee, 20-22 December, 2018.

Sharma, V., Shrimali, M., Bharti, S. and Datta, T. (2019), "Seismic energy dissipation in semi-rigid connected steel frames", *Proceedings of the 16th World Conference on Seismic Isolation, Energy Dissipation and Active Vibration Control of Structures*, Saint Petersburg, Russia.

Sharma, V., Shrimali, M.K., Bharti, S.D. and Datta, T.K. (2019). "Sensitivity of lateral load patterns on the performance assessment of semi-rigid frames", *Proceedings of the 7th Nirma University International Conference on Engineering (NUiCONE 2019), November 21-22, 2019*, Ahmedabad, India, July 3, 2020.

Sharma, V., Shrimali, M.K., Bharti, S.D. and Datta, T.K. (2020), "Behavior of semi-rigid steel frames under near- and far-field earthquakes", *Steel Compos.Struct*., **34**(5), 625-641. https://doi.org/10.12989/scs.2019.34.5.625

Silva, A.R.D., Batelo, E.A.P., Silveira, R.A.M., Neves, F.A. and Gonçalves, P.B. (2018), "On the nonlinear transient analysis of planar steel frames with semi-rigid connections: From fundamentals to algorithms and numerical studies", *Latin Am. J. Solids Struct*., **15**(3), 1-29. https://doi.org/10.1590/1679-78254087.

SP-6-1 (2003), "SP-6-1 Handbook for Structural Engineers -Part-1 Structural Steel Sections".

CC

Annexure 1: Abbreviations

α	Stiffness parameter for semi-rigid connection	NSA	Nonlinear static analysis
β	Strength Parameter for semi-rigid connection	NTHA	Nonlinear time history analysis
T_d	Target displacement	MR	Moment resisting
E_{rms}	Error in root mean square value	PGA	Peak ground acceleration
IDR_{max}	Maximum inter-story drift ratio	FF	Far-field
BS_{peak}	Peak base shear	NF-D	Near-field with directivity effect
PSD	Peak top-story displacement	NF-F	Near-field with fling-step effect
SRSS	Square root of the sum of squares	POA	Pushover Analysis
		SR	Semi-rigid